AUTOMATED SEGMENTATION OF TUMOUR CHANGES IN TEMPORAL PET-CT DATA

Goodal Nyirenda[1], Jinman Kim[1], Lingfeng Wen[1, 2] and David Dagan Feng[1]

[1]School of Information Technologies, Faculty of Engineering & Information Technologies, University of Sydney, NSW 2006, Australia
[2]Department of PET and Nuclear Medicine, Royal Prince Alfred Hospital, Missenden Road, Camperdown, NSW 2050, Australia

ABSTRACT

Positron emission tomography and computed tomography (PET-CT) is widely accepted as the best imaging in the management of cancer. To assess response to treatment, multiple scans of a patient are usually acquired and tumour changes are analysed at different stages during the treatment. However, it is difficult to assimilate these changes, especially where a patient has in excess of e.g. four temporal scans. We aimed to advance current single-time PET tumour segmentation algorithms to multiple-time PET studies. We therefore proposed a new treatment response confidence connected region growing (TRCCRG) algorithm. Our algorithm is interactive and includes a combined function of Radial profile plot and Rodbard curve fitting as a measure of tumour likelihood for the morphologically expanded volume in successive scans. Evaluation with 10 simulated PET data and 6 clinical lymphoma PET-CT patients (each with 4 studies) demonstrated that the proposed method was successful in detecting and delineating tumours.

Index Terms— Adaptive region growing, PET-CT segmentation, Treatment response, Tumour changes.

1. INTRODUCTION

PET-CT, which combines Positron Emission Tomography (PET) and Computed Tomography (CT), has been widely accepted as the best imaging in the management of cancer, such as initial diagnosis, re-staging and evaluation of treatment response, due to its unique ability to visualize metabolic function from PET data supplemented with co-registered anatomical CT information [1-3]. For example, in the treatment of lymphoma, patients often have multiple scans for evaluating treatment response and monitoring potential recurrence. Fig.1 gives an example of initial and subsequent follow-up PET-CT studies for a patient with lymphoma. The high volume of images, (> 300 axial slices for one study), and subsequent multiple studies, have given rise to better understanding of the progression of tumours and in providing best treatment options. However, the high volumes of images also pose a challenge for accurate and efficient image analysis and processing. It is very difficult to trace the changes of multiple tumours and perform quantitative assessment of their changes over time.

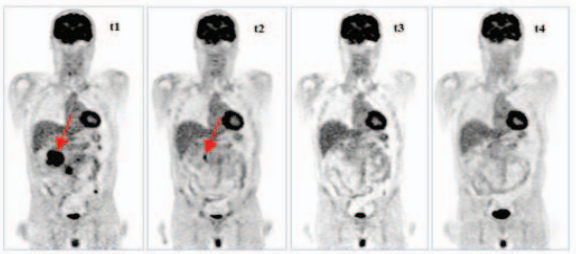


Figure 1. A patient study showing good response to treatment with tumours in the abdomen visible in the 1st scan (t_1) receding to a smaller tumour in t2 followed by no visible tumours in $t_3 - t_4$.

There are many researches done for tumour delineation [4-10]. Hatt et al. [5] developed a fuzzy local adaptive Bayesian (FLAB) clustering algorithm and was shown to be effective for small and heterogeneous tumours. In another clustering approach, Belhassen and Zaidi [6] presented a Fuzzy C-means (FCM) algorithm for PET, combing spatial information of the neighboring voxels derived from the Wavelet domain. As an alternative to clustering, Hua et al. [7] proposed an adaptive region growing (RG) algorithm with the dual-front active contour model for tumour segmentation. Recently, Ballangan et al. [8] presented a 'downhill' RG algorithm optimized for lung cancer tumour segmentation, where the intensity gradient of voxels was used to classify the voxels belonging to the tumour. In another study, Day et al. [10] introduced an adaptive RG based on the mean and standard deviation of voxel intensities to iteratively delineate the tumours. There are some recent studies that investigated the use of segmentation in temporal PET studies. David et al. [11] develop a fusion method using multi-observation Bayesian framework to evaluate tumour volume and uptake changes in temporal PET scans. Opfer et al. [12] also presented a tumour tracking algorithm for temporal PET/CT scans by combining rigid registration, block matching and region growing methods.

In our study, we aimed to improve the current lesion segmentation algorithms for single-time PET study to

multiple-time PET studies of the same patient. We therefore proposed a new treatment response confidence connected region growing (TRCCRG) algorithm. Our algorithm extends upon Day's confidence connected region growing (CCRG) algorithm [10] with a combined function of the Radial profile plot and the Rodbard curve fitting to measure the likelihood of tumour changes among the temporal scans.

2. METHODOLOGY AND MATERIALS

2.1. Methodology

Our proposed algorithm integrates tumour delineation and tumour tracking with the major processes shown in Fig 2.

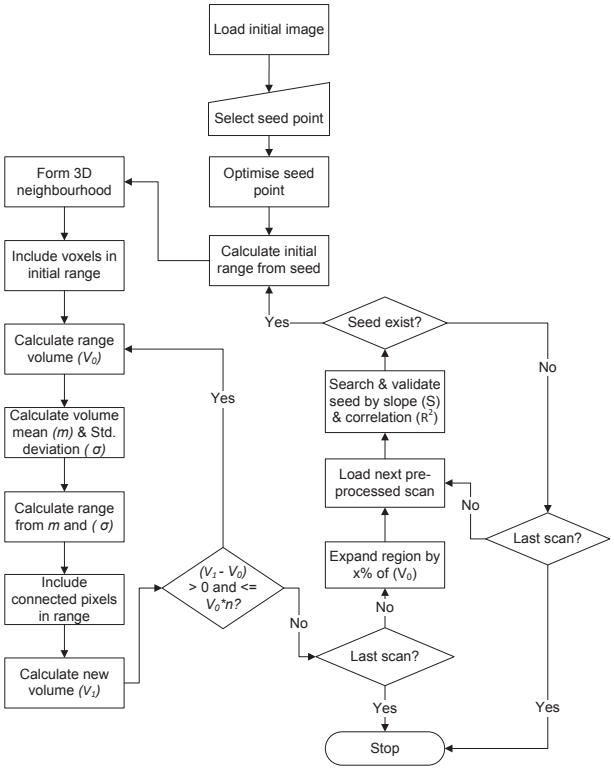


Figure 2. Flow diagram showing major processes of our proposed TRCCRG temporal PET-CT segmentation algorithm.

2.1.1. Tumour segmentation

Our algorithm begins with tumour segmentation in the first PET-CT image. Upon selection of a seed point by a mouse click (user-interaction), the algorithm calculates an initial segmentation iteration range, using 10% of the seed's intensity value as the threshold. The algorithm uses a 3D neighbourhood for voxel analysis defined by $2r + 1$ where r is a radius factor that can be chosen by the user and was empirically set to 3. Successive iterations of the algorithm are based on the new range that is calculated from the average (m) and standard deviation (σ) of the grown region (volume). The range calculation uses a factor f that can be adjusted depending on the image modality characteristics. In our case the factor was empirically set to 2.5 and an iteration stopping criteria was empirically set to n times initial volume where n ranges from 1 to 10 depending on the tumour volume. Any voxel V from an image I that falls within the new range is taken as part of the tumour and added to the tumour volume. Using I and V, the confidence voxel intensity interval range can be represented by:

$$I(V \in [m - f\sigma, m + f\sigma]) \quad (1)$$

2.1.2. Tumour tracking

We automatically align the temporal scans using non-rigid B-spline registration as presented by Kim et al. [13]. To address the possibility of the same tumour having grown off the initial point in the successive scans, the algorithm creates an expand volume for the new seed search. The expanded volume is created proportionally through increasing the initial delineated volume (V_0) by 30%, using image morphology (Fig. 3).

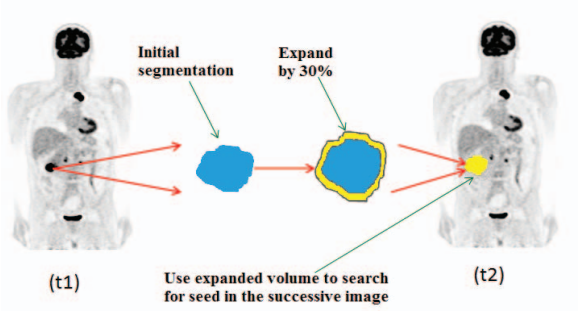


Figure 3. Initial segmented volume in t_1 and the expanded volume in the successive scan t_2.

The seed points in successive images (time point t) are selected based on the expanded volume of the tumour in the previous image (time point t-1). The seed point is selected from the successive image only if it satisfies the following four criteria: (i) the seed point is within an expanded search region, (ii) the seed point has the maximum intensity within the expanded region, (iii) the new seed region of interest that is created from the expanded region in successive scans has a radial plot with negative slope ($S = \Delta y/\Delta x$) of < -20, and (iv) the radial plot in (iii) above has a Rodbard curve fitting correlation (R^2) of more than 95%.

After obtaining candidate seed's intensity and location in the successive scans, we need to evaluate whether the candidate seed belongs to the tumour or not. To solve this problem we analyse the pixels in the expanded region using a radial profile plotter. The radial profile plotter creates a line graph, of the average pixel intensities around concentric circles in an image as a function of the location distance from the centre of the circle to the reference pixel in the object.

Our algorithm is designed to use the radial profile plotter in tracking tumours that are circular in shape. The slope of the

graph from the radial profile is not enough to determine the presence of the tumour in the region. A situation may arise where the graph has an adequate slope but the intensity does not gradually decrease from the centre to the edge of the region. Curve fitting is thus used to define the degree of smoothness of the gradual decrease of the pixel intensities. Our algorithm uses the Rodbard function for curve fitting which demonstrated consistent slope characteristics to what we observed in our data sets. Rodbard function produces a sigmoidal voxel intensity graph [14] with four parameters:

$$y = d + (a - d)/(1 + (x/c)^b) \quad (2)$$

where parameters a and d define the upper and lower asymptotes of the curve respectively, parameter c is the dilution associated with the point of symmetry of the sigmoid and parameter b represents the curvature of the curve which is related to the slope of the curve.

2.2. Materials

2.2.1. Simulation data set

We used the simulation Lymphoma PET image available from OncoPET database [15]. The reconstructed PET image was 192×96×243 voxels in dimension with isotropic voxels of 3.57×3.57×3.57 mm^3. From this simulated database, we selected 10 images that were arranged into temporal scan groups. The first 2 groups had 3 images per group with good response; the third group had 4 images with poor response; and the last two groups had 3 images per group with no changes in tumour volume over time.

2.1.1. Clinical data set

The clinical images used were whole-body FDG PET-CT scans obtained on a Siemens Biograph TruePoint scanner with PET resolution of 168×168 pixels at 4.07×4.07mm and CT resolution of 512×512 pixels at 0.98×0.98mm. The scans were sequentially acquired and were hardware co-registered. The slice thickness was 3.0mm for both modalities. The PET and CT images were re-sampled to equal dimensions of 256×256 pixels at 1.98×1.98mm. The test data consisted of 24 PET-CT lymphoma studies of 6 patients, each patient with 4 temporal scans, with varying level of response to treatment. Clinical diagnostic reports were used for comparative evaluation.

3. RESULTS AND DISCUSSION

Simulation and clinical studies were used to measure the effectiveness of our algorithm in its ability to delineate and track tumour changes. Simulation was used to create our test cases to quantitatively assess our algorithm performance whereas the clinical images, with large tumour size/shape variation as well as greater diversity in tumour changes in temporal scans, was used to demonstrate the potential clinical applications. In the clinical images, we selected tumours that had circular shapes but the size of the tumours varied greatly.

3.1. Simulation results.

The algorithm successfully detected and tracked tumours in all the 10 simulation images as shown in Table II.

Table II. Summary of the simulation test results

GROUP ID	IMAGE NUMBER/VOLUME	COMMENT
S1	t_1 (123 voxels), t_2 (65 voxels), t_3 (0 voxels)	Detected and delineated in t_1 and t_2. Detected as no tumour in t_3. Good response.
S2	t_1 (65 voxels), t_2 (123 voxels), t_3 (0 voxels)	Detected and delineated in t_1 and t_2. Detected as no tumour in t_3. Good response.
S3	t_1 (57 voxels), t_2 (244 voxels), t_3 (244 voxels), t_4 (370 voxels)	Detected and delineated in t_1 to t_4. Poor response where $t_n >= t_{n+1}$
S4	t_1 (63 voxels), t_2 (60 voxels), t_3 (67 voxels)	Detected and delineated in t_1 to t_3. Poor response.
S5	t_1 (67 voxels), t_2 (63 voxels), t_3 (60 voxels)	Detected and delineated in t_1 to t_3. Poor response.

The algorithm was able to track tumours in the successive scans when the tumor was fully or partially within the expanded volume. For the tumour that was partly outside the expanded region, the algorithm managed to detect and segment the entire tumour including the voxels outside the expanded volume. Fig 4 presents a visual representation of one of the tumours tracked over three images.

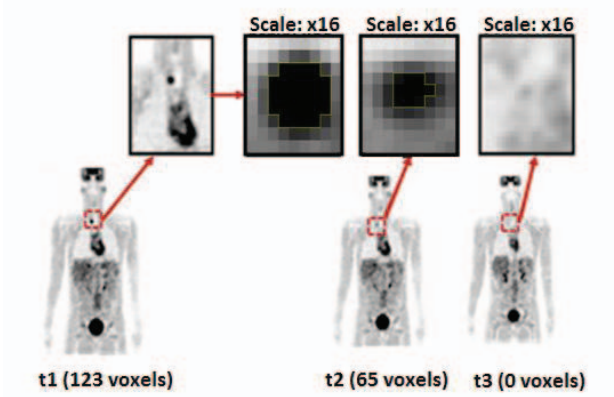


Figure 4. Results of a simulation data (S1 from Table II) showing positive treatment response with decreasing tumour size.

3.2. Clinical results.

Our algorithm successfully tracked and delineated tumours for all 7 cases among 6 patients as in Table III. Fig. 5 is an example where the tumour in the superior mediastinum, though decreasing in volume, is persistent in t_2 to t_4 with

sizes of 650, 353 and 263 voxels, respectively. Moreover, tumour in the abdomen was also segmented correctly over the temporal scans.

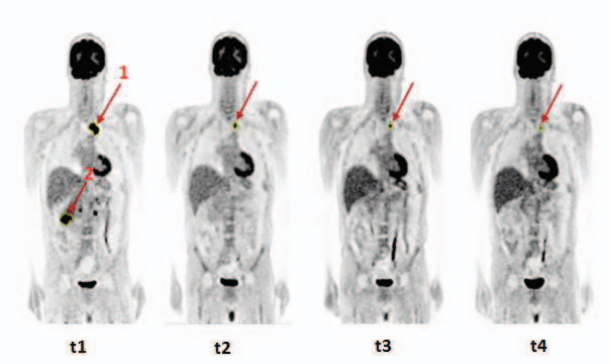


Figure 5. Results of tumour 1 segmentation on patient 1 (P1). In t_1, segmentation of the tumour in the superior mediastinum (arrow 1) and a secondary tumour in the right side of the abdomen (arrow 2) is clearly visible. The successive scans in t_2 to t_4 shows that the tumour in the abdomen is removed (good response) while the other tumour is consistent among all the scans (poor response).

Table III. Summary of the clinical test results

PATIENT ID	CLINICAL REPORT	OBSERVATION/ RESULTS
P1	Tumour 1 persistent through t_1 to t_4	Detects and delineates in t_1 to t_4
	Tumour 2 disappears in t_2 to t_4	Reports no tumour in $t_2 - t_3$
P2	Good response, no tumour in t_2 to t_4	Delineates in t_1, reports non in t_2 to t_4
P3	Good response, no tumour in t_2 to t_4	Delineates in t_1, reports non in t_2 to t_4
P4	Persistent, tumour reappear in t_4	Reports none in $t_2 - t_3$, delineates in t_4
P5	Good response no tumour in t_2 to t_4	Delineates in t_1, reports non in t_2 to t_4
P6	Good response no tumour in t_2 to t_4	Delineates in t_1, reports non in t_2 to t_4

The average computation time for our algorithm using the clinical data of four temporal scans was 100.8 seconds (±50 sec) running on Intel Core i7 (3.20GHz), 8GB RAM on 64-bit Windows7. The large time variation is due to the tumour changes; if there are no tumours to segment due to good response, the computation is reduced. The algorithm was able to successfully detect tumours in successive scans that had different voxel intensities (lower or higher) as compared to the initial tumours. The algorithm was also able to detect a tumour that had changed the initial location but was within the expanded region for the clinical data (P4). We selected tumours that were circular in shape because the use of radial profile plot does not produce descriptive results for non-circular tumours.

4. CONCLUSIONS

This research developed an algorithm that detects, delineates and tracks tumour changes in temporal PET-CT scans. Radial profile plot and curve fitting, when used in conjunction with adaptive region growing, proved to work robustly in detecting the changes in tumour volume in our simulation and clinical temporal scans. We will further study our algorithm with larger variation of tumour types.

5. REFERENCES

[1] V. Kapoor, et al., "An introduction to PET-CT imaging," *Radiographics*, 24:523-43, 2004.

[2] H.S. Lim, et al., "FDG PET/CT for the detection and evaluation of breast diseases: usefulness and limitations," *Radiographics,* 27(Suppl 1): S197-S213, 2007.

[3] C. K. Hoh, et al., "Whole-body FDG-PET imaging for staging of Hodgkin's disease and lymphoma" *J. Nucl. Med*., 38:343-348, 1997.

[4] H. Zaidi & I. El Naqa, "PET-guided delineation of radiation therapy treatment volumes: a survey of image segmentation techniques," *Eur. J. Nucl. Med. Mol. I.*, 37:2165-87, 2010.

[5] M. Hatt, et al., "A Fuzzy Locally Adaptive Bayesian Segmentation Approach for Volume Determination in PET," *IEEE Trans. Med. Imag.,*28:881-93, 2009.

[6] S. Belhassen and H. Zaidi, "A novel fuzzy C-means algorithm for unsupervised heterogeneous tumor quantification in PET", *Med. Phys.*, 37: 1309-24, 2010.

[7] L. Hua, et al., "A novel PET tumor delineation method based on adaptive region-growing and dual-front active contours", *Med. Phys.*, 35:3711-21, 2008.

[8] C. Ballangan, et al., "Automated Delineation of Lung Tumors in PET Images Based on Monotonicity and a Tumor-Customized Criterion", *IEEE Trans. Info. Tech. Biomed*., 691-702, 2011.

[9] L. A. Drever, et al., "Comparison of three image segmentation techniques for target volume delineation in positron emission tomography", *J. Appl. Clin. Med. Phys.*, 8:93-109, 2007.

[10]E. Day, et al., "A region growing method for tumor volume segmentation on PET images for rectal and anal cancer patients", *Med. Phys*., 36:4349-58, 2009.

[11]R. Opfer, et al., "Automatic lesion tracking for a PET/CT based computer aided cancer therapy monitoring system" in Med. Imaging: 6915:91513-1-9, 2008.

[12]S. David, et al., "Multi-observation PET image analysis for patient follow-up quantitation and therapy assessment," Phys. Med. Bio., 56, pp. 5771-88, 2011.

[13] J. Kim, et al., "Visual tracking of treatment response in PET-CT image sequences," *IJCARS*, 6:S17-S18, 2011.

[14]G. M. Carlone, et al., "Comparisons of standard curve-fitting methods to quantitate Neisseria meningitidis group A polysaccharide antibody levels by enzyme-linked immunosorbent assay," *J. Cli Microb.* , 29:1439-1446, 1991.

[15]S. Tomei, et al., "OncoPET_DB: A Freely Distributed Database of Realistic Simulated Whole Body 18F-FDG PET Images for Oncology," *IEEE Trans. Nuclear Science,* vol. 57, pp. 246-255, Feb 2010.